Full length article

Concordant element of the oxidation kinetics—Interpretation of ellipsometric measurements on Zr

Alekszej Romanenko [a,b], Emil Agócs [b], Zoltán Hózer [b], Peter Petrik [b,*], Miklós Serényi [b]

[a] Doctoral School of Chemistry, Eötvös Loránd University, Pázmány Péter sétány 1/A, H-1117 Budapest, Hungary
[b] Centre for Energy Research, Konkoly-Thege Rd. 29-33, 1121 Budapest, Hungary

ABSTRACT

In this study we report on the growth of ZrO_2 films upon the gradual thermal annealing of Zr in the temperature range of 500–700 K. The thickness of the oxide was monitored by in-situ spectroscopic ellipsometry with temporal and thickness resolutions of a few seconds and a few nanometers, respectively. A remarkable feature of the process was that the growth of the oxide can be terminated immediately when decreasing the temperature by a few K. This suggests that, in addition to the driving force, a built-in control adjusts the final thickness determined only by the temperature in sync with the formation and growth of dense oxide films. The derived phenomenological model includes the concept of a 'depletion layer' known from semiconductor physics. The validity of the model and the pressure dependence of oxidation is discussed.

1. Introduction

The first of oxide growth models originate from Wagner's assumption that metal oxidation takes place by diffusion of charged particles and is valid for thick film growth ($x > 1$ μm) at high temperatures [1]. By raising a linear diffusion equation, which incorporates the electric field across semiconducting passive oxides, Wagner found that the film growth is parabolic [2]. Cabrera and Mott developed another approach where an electric field (Mott potential) controls the diffusion of ionic point defects necessary for oxidation [3]. They suggested in 1949 that thin film growth was directly dependent on the migration of interstitial cations where the rate limiting step is cation injection at the metal/film interface. Cabrera and Mott's solution for thin film growth at low temperatures has an inverse logarithmic law of growth. Afterwards, the oxidation kinetics of Cu thin films in the temperature range of 100–300 °C for film thicknesses between 20 and 150 nm was investigated and found to follow a linear rate law, which indicates that the oxidation process is surface reaction controlled [4]. The oxidation of thin films of other metals, e.g. Ni, Cr, Co, Al, and Si, typically exhibit a parabolic growth rate for similar oxidation conditions, characteristic for a diffusion-controlled oxidation process [5]. There have been numerous studies conducted on Zr [6–8]. In many cases, these resulted in the determination of material parameters, such as the diffusion coefficient [9–11].

Most studies deal with either the initial [12–14] or final [11,15] stages of the Zr oxidation. The initial stage of oxidation starting from a clean crystalline surface in ultra-high vacuum studied by a combination of in-situ spectroscopic ellipsometry (SE) and X-ray photoelectron spectroscopy (XPS) is a well-defined and well-controlled process that allows the in-depth understanding of the growth of the first few nanometers [4,16–18]. The final stage [11] that leads to the peel-off [19] of the layer has a significance for material degradation in the nuclear power plant technology. The different stages of Zr oxidation have phenomenologically been characterized by subsequent linear [12], parabolic [11] and cubic phases terminated by a final linear phase [9] that may lead to breakaway [19–21], depending on the alloy composition [11,15]. The pioneers of Zr oxidation have been followed by many investigations dominated by gravimetry [8,11,19] for the characterization of the amount of growing oxide in the thickness range from a few micrometers to hundreds of micrometers [10].

There were only a few studies, including our group [22,23] that have dealt with the optical thickness measurements of the oxide, but they mainly used ex-situ characterizations on thin films [24], with some exceptions including measurements during electrochemistry [25,26]. Furthermore, all the above studies are on thicknesses up to a few nanometers, or in the micrometer range. The range between a few nanometers and a few hundred nanometers is unexplored, especially using in-situ optical characterization. Ex-situ optical investigations are

---

of significant importance for the development of optical models and determination of optical constants [27,28]. Here we utilize the capabilities of SE for the in-situ characterizations with thickness and temporal resolutions in the range of nanometers and seconds, respectively. These features allow the development and verification of an oxidation model for the thickness range of a few hundred nanometers. We focus on an alloy that is relevant in the nuclear power plant technology, and do not discuss the composition-dependent oxidation properties [29–31]. The material we use in this study is sufficient for the demonstration of the proposed oxidation model. A greater knowledge of the oxidation process in this regime is of primary importance in many applications including nuclear technology [19] and microelectronics [32].

2. Material and methods

2.1. Sample preparation

Zr plates in sizes of approximately 20 mm by 10 mm made of an E125 alloy (2.45% Nb, 0.035% Fe and 0.069% O [33]) have been prepared. The samples have been polished with diamond paste to such an extent that only a few nanometers of residual oxide was observed by ellipsometric spectra.

2.2. Annealing

The Zr samples were annealed in an isolated quartz tube shown in Fig. 1A. Argon and Ar/O$_2$ gas mixtures with O$_2$ partial pressures of 0, 1.25, 5 and 20% were flowed at atmospheric pressure. A ceramic plate is mounted in the tube so that the surface of the samples placed on the ceramic plate coincides with the axis of the tube. This configuration enables the ellipsometry measurement to be performed at any angles of incidence that is allowed by the equipment (45–90°). The heat cell was placed at the stage of the ellipsometer. The standard alignment procedure can be performed also through the tube that makes an automatic sample alignment possible. The measurement spot was focused to make sure that the beam enters the tube perpendicular to its surface over the whole spot which has a diameter of approximately 3 mm outside of the tube, and a spot of approximately 0.3 mm × 1.0 mm on the surface of the sample.

The plate can be heated up to 873 K. The precision of the temperature control is approximately 0.1 K. In this experiments the temperature was increased at a rate of 10 K/min and it was kept at given temperatures until a nearly saturated thickness was reached. Then the temperature regulator was turned off for 30 s to drop the heat level. By doing so the growth of the oxide layer immediately stops. These extra steps were added to support our assumptions about the kinetics of layer growth. After that a new ramp up was started to the next temperature. The thickness was determined by ellipsometry in real-time during annealing, to have a precise control of the annealing times.

2.3. Measurement

The optical measurements were made by a Woollam M-2000DI rotating compensator spectroscopic ellipsometer at the angle of incidence of 70° with temporal resolutions of a few seconds and thickness resolution under 1 nm. Ψ and Δ spectra were recorded and evaluated real-time in every 10 s during annealing, where the complex reflection coefficient is $\rho = |\tan\Psi|\exp(i\Delta)$. Typical spectra measured on a sample oxidized at 700 K is shown in Fig. 1(B). Multiple-angle measurements were made before annealing to help building a precise optical model used during the real-time investigations. The measurement through the tube makes no aberration of the SE spectra, which was verified by the characterization of thermal oxide-covered reference Si wafers. The 10 s cycle of data acquisition was selected to be large enough to decrease noise, but small enough to precisely follow the changes during measurement.

3. Theory

3.1. Model of oxidation

The concept of diffusion-controlled growth assumes the formation of dense oxide films on the metal surface by diffusion of O$^-$ through the oxide layer under the influence of a strong concentration gradient around the interface. All the free oxygen atoms migrate to the oxide-metal interface and react with the metal. The rate of this incorporation process depends on the reaction rate coefficient of k_{exp}. The initial components (Zr$^+$ cations and O$^-$ anions) of the reaction are practically in equilibrium, and under a certain time the reaction provides the final product (ZrO$_2$). However, because the anions move to the metal surface and take part in the reaction, they leave a positively charged region behind. This process continues until the region has an electrical charge large enough to repulse the cations to enter the vicinity of the oxide-metal interface. Eventually, a state of equilibrium will occur producing a "potential barrier" zone. Since no free anion can rest in a potential barrier zone, the region becomes completely depleted, and the oxidation process is stopped. This area is called the "depletion layer" known from semiconductor physics, and the thickness (w) of the layer is proportional to the square of the potential [34].

Based on the above considerations, several sufficient assumptions should be made to create a reasonable model: (i) No diffusion of cations and electrons in the oxide film are considered. (ii) The diffusion of atomic oxygen in the oxide film happens via the vacancy and interstitial mechanism. (iii) Dissociation and ionization mechanism of oxygen molecules is not involved. (iv) The existence of a few nm oxide layer is assumed, i.e., the oxide growth is considered to be in the form of an additional layer.

In the initial equations, we take into account two observations by ellipsometry. First, the growth process can be stopped by reducing the temperature by a few degrees. This condition appears to be stable according to the observations. It means that a given flux (J) delivering O$^-$ at a concentration of c can provide anions in a quantity sufficient to develop (presumably stoichiometric) oxide in a volume of ΔV during the time τ. This flux penetrates the previously formed oxide with practically no modification of the layer. Therefore, the dependence on the oxide thickness at the O$^-$ inflow side (x, Fig. 2) does not need to be assumed. If the flux J (in units of mol/(nm^2 s)) enters the cross section of A during a time period of τ, the following equation holds:

$$\tau J A = c\ \Delta V, \tag{1}$$

where ΔV denotes the volume. During the oxidation process ZrO$_2$ forms with a reaction rate coefficient of k_{exp} detected during the experiment, and an oxygen concentration of $c_0 = 9.13 \cdot 10^{-19}$ mol/nm^3. At this point, we can assume that the reaction proceeds according to the law of Arrhenius. Consequently, it has the form of $k_{exp} = k_0 \exp(-E_a/(k_B T))$. Here, k_B and E_a denote Boltzmann's constant and the activation energy of the process, respectively, and k_{exp} can be determined from the experiment:

$$\tau k_{exp} = c_0 \Delta V. \tag{2}$$

Combining the two equations the flux takes the temperature dependent form of

$$J = J_0 \exp\left(-\frac{E_a}{k_B T}\right) \tag{3}$$

with

$$J_0 = \frac{k_0}{A} \cdot \frac{c}{c_0}. \tag{4}$$

The second observation from the heat treatment experiment is that the thickening of the oxide continues at a new, higher temperature. Thus, the oxide layer can be constructed gradually from practically microscopically thin layers. We can suppose that there must be a sudden change in the oxide concentration at the metal oxide transition.
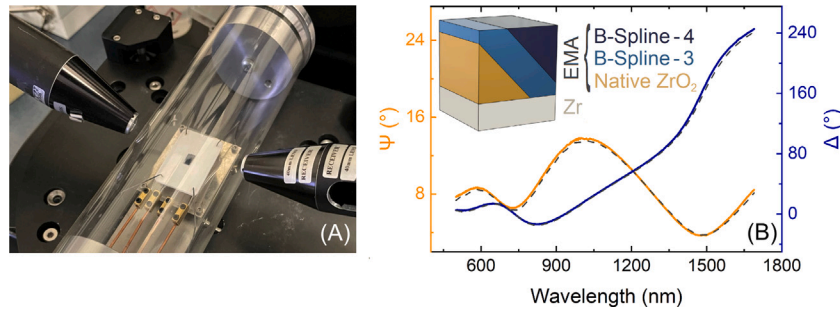
Fig. 1. (A) The heat cell constructed for multiple-angle SE measurements in controlled ambient and temperature. (B) Typical measured (solid lines) and fitted (dashed lines) SE spectra on the sample oxidized at 700 K for 18000 s. The inset shows the optical model used for the evaluation of the SE spectra. The different components of the EMA layer were determined from different stages of the oxidation: the initial native zirconium oxide (yellow), a B-spline-3 fitted after the third heat-step 618 K (light blue) and a B-Spline-4 fitted after the fourth-final 700 K step (dark blue).
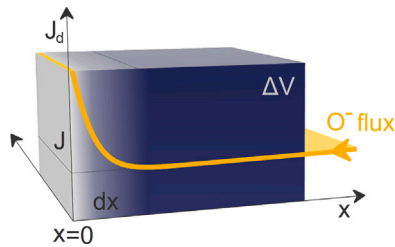

Fig. 2. Schematic diagram of the kinetic model. The yellow curve shows the anion flux (J_d) as a function of depth. The $x = 0$ position corresponds to the interface between the oxide and the substrate.

According to Fick's first law, the flux is proportional to the negative of the concentration gradient at each point; this results practically in a singular value of the anion flux. We specify an identical area, A, on each plane of dx in Fig. 2, and we can calculate the number of oxygen atoms that are added to the volume between the two planes during an increment of time, dt:

$$(J_d - J)A dt = c_0 A dx. \tag{5}$$

Here, J_d is considered to be the charge carrier transport, analogous to that used in calculations for semiconductors. It depends on the mobility (μ) and the electric field (E):

$$J_d = c_0 v_d = c_0 \mu E, \tag{6}$$

where the velocity of the anions is $v_d = \mu E$.

$E(x)$ can be determined in a way similar to the physics of semiconductor p–n junctions (using the Boltzmann limit instead of the Bose–Einstein statistics), assuming $c(x) = c_0 x/w$ at the metal-oxide interface. In order to determine $J_d(x)$, we are searching for $E(x)$, which can be expressed as a function of the potential (U):

$$E = -e \frac{\partial U}{\partial x}, \tag{7}$$

where e denotes the elementary charge. Recalling the laws of statistical mechanics, we can write the concentration of oxygen anions near the $x = 0$ transition:

$$\frac{c(x)}{c_0} = \exp\left(-\frac{eU}{k_B T}\right), \tag{8}$$

$U(x)$ can be expressed as

$$-eU = k_B T \ln\left(\frac{c(x)}{c_0}\right), \tag{9}$$

the derivative of which is

$$e \frac{\partial U}{\partial x} = -\frac{k_B T}{x}. \tag{10}$$

Substituting $E = -e \partial U / \partial x$ into Eq. (6), J_d can be expressed as

$$J_d = c_0 \mu E = c_0 \mu \frac{k_B T}{x} = \frac{c_0 D}{x} = \frac{L}{x}. \tag{11}$$

In this formalism $v_d = \mu k_B T/x$ is the drift velocity, and $D = \mu k_B T$ is the Stokes–Einstein formula for the Brownian motion. Also note that $k_B T/x$ is the force (in N) applied to the anions by the electric field. The mobility (μ), which is the inverse of the friction constant, is related to the fluctuation of the velocity of the Brownian motion, being a manifestation of the fluctuation–dissipation theorem [35]. The mobility (μ) in the diffusion coefficient (D) is a function of the temperature, and here interstitial diffusion can also be taken into account if we arbitrarily supplement it with the usual exponential formula:

$$L = c_0 \mu \, k_B T \, \exp\left(-\frac{E_d}{k_B T}\right). \tag{12}$$

Substituting the results into Eq. (4), taking into account the direction of flow regarding the coordinate system of Fig. 2:

$$\frac{L}{x} - J = K \frac{dx}{dt}. \tag{13}$$

Here, instead of concentration c_0, we introduce a parameter K, suggesting that in general cases it may be a nonstoichiometry value. The integration of Eq. (13) from 0 to t results in

$$t = -x \frac{K}{J} - \frac{LK}{J^2} \ln\left(1 - x \frac{J}{L}\right). \tag{14}$$

Eq. (14) describing the time dependence of oxide growth contains an important statement; the numerous of the logarithm function can only be interpreted in the range 0 and $x = \frac{L}{J}$, which means that the layer thickness approaches a δ value at a given temperature, where

$$\delta = \frac{L}{J}. \tag{15}$$

Also the Eq. (14) can be simplified using a series expansion at $x \simeq 0$ as follows:

$$t = \frac{K}{2L} x^2, \tag{16}$$

4. Results

4.1. Model of the optical measurements

To build proper SE models, the experience and result from previous investigations [22,23] were utilized. The choice was settled on a one-layer model, which was used with an effective medium approximation (EMA) model for the surface layer, whereas the substrate was described by Lorentz oscillators. In the EMA layer the dielectric function of the surface layer (parameterized by the B-Spline model [36,37]) at different stages of the oxidation were mixed: the initial native oxide, a B-spline-3 fitted after the third 618 K heat-step and a B-Spline-4 fitted after the fourth-final 700 K step, as shown in Figs. 1(B) and 3.

The gained refractive indices and few relevant Refs. [32,38–40] can be also seen in Fig. 3. During oxidation only the thickness and the volume fractions of the components were fitted, taking into account the structure-dependent optical properties of the film [24,41,42]. The surface roughness was neglected, which is in this case part of the layer, possibly causing and offset in the layer thickness on the nm scale. Compared to the thicknesses of the order of 100 nm, and due to the fact that we were primarily looking for the dynamics of the thickness change, this effect is expected to be negligible.

4.2. Analysis of the optical measurements

The kinetic curves of Figs. 4 and 5 described by Eq. (14) were fitted using Eq. (15) and the following substitution:

$$\frac{K}{J} = \alpha, \tag{17}$$

Using this notations, Eq. (13) takes the normalized form of

$$\frac{\delta}{x} - 1 = \alpha \frac{dx}{dt}. \tag{18}$$

The Eq. (18) expresses that the oxide stops growing at the thickness of $x = \delta$. The α parameter illustrates the reciprocal of the growth rate of the oxide layer. The value of this and the δ thickness can be well matched in the range of 300–600 K based on the measurement results:

$$\alpha = 16.4 \exp\left(\frac{0.96}{k_B}\left[\frac{1}{T} - \frac{1}{\theta}\right]\right) \tag{19}$$

in unit of s/nm, where $\theta = 666$ K is included in the formula to remind us of the range of validity of the formula,

$$\delta = 0.47 \, T \exp\left(\frac{-0.47}{k_B}\left[\frac{1}{T} - \frac{1}{\theta}\right]\right) \tag{20}$$

in unit of nm.

The oxidation process described by the equation takes place under extremely strictly defined conditions. It should first be mentioned that the variable x in the equation is only interpreted at positive values. It ignores the processes (thus diffusion of metal ions) within the metal surface. All this is consistent with the fact that our goal in this study is to demonstrate the interpretation of the data measured by ellipsometry.

Second, we emphasize that the equation describes the process such that each O⁻ anion incorporates into the solid oxide. This incorporation takes place only at the metal oxide interface ($x = 0$). The fact that there is always enough oxygen in atomic form is due to the thermodynamic description of the equilibrium of metal oxidation. The model assumes that the growth rate determined and measured by the reaction constant k_{exp} receives sufficient replenishment from the flux J. If the drift velocity v_d is less than the growth rate, the growth of the oxide layer will be stopped. This experiment proves that with a small decrease in temperature, the growth breaks off immediately.

5. Discussion

The in-situ measurement demonstrated that the observed relation of the oxide growth agrees well with our formulas in the temperature range of 300–600 K. Measurements taken up to 600 K can be fitted in an acceptable accuracy, but the form of the growth profile recorded at 700 K is surprisingly different from the others. We are not aware of such a rapid, phase-transition-like change within a given system, so we try to provide the explanation with the model itself. To do this, we first interpret the flux J as follows. By substituting $x = \delta/2$ into Eq. (18) we obtain

$$1 = \alpha \frac{dx}{dt}, \tag{21}$$

or using Eq. (17)

$$J_0 \exp\left(\frac{-E_a}{k_B T}\right) = K \frac{dx}{dt}. \tag{22}$$

This means that J is numerically equal to the incoming O⁻ anion flux that the layer absorbs when it reaches half of the predictable oxide thickness (δ — see the Eq. (20)). By studying Eq. (18), it becomes clear that in the later phase of growth, the value of the absorbed flux decreases to zero, where the oxidation process terminates. In the earlier stage – when starting the annealing J_d – must approach an infinitely large (singular) value at $x = 0$. It should be noted that the approximation to describe the initiation of growth, $x \approx 0$, can be easily calculated by omitting the value of 1 in Eq. (18), since its value is negligible to δ/x. According to Eq. (6) the flux $J_d = v_d c_0$ and the product of $v_d c_0$ must be near constant in the middle range of the oxide layer. Thus, the incoming flux demands J of the oxidation at temperature T reaching a thickness of $x = \delta/2$ an essential feature of the process.

Furthermore, consider how much flux J_{ox} produces depending on the partial pressure of oxygen in the environment. Under our conditions of temperature and pressure, oxygen behaves qualitatively like an ideal gas, thus a very rough estimation can be made of the particle flux J_{ox} reaching the surface of the oxide boundary is

$$J_{ox} = \frac{p}{2\sqrt{3k_B T m_0}}, \tag{23}$$

where p denotes the partial pressure in Pascal and m_0 stands for the mass of oxygen atoms (no dissociation was considered). It can be seen from the table that at normal pressure and low temperature the number of available oxygen atoms exceeds J, which determines the oxidation process. The oxygen demand of the system can be characterized by a pressure value p^*. This is determined from the equality of J and K disregarding all kinds of dissociation efficiencies and diffusion losses:

$$J_0 \exp\left(\frac{-E_a}{k_B T}\right) = \frac{p^*}{2\sqrt{3k_B T m_0}}, \tag{24}$$

It can be seen that as the temperature increases, the number of available oxygen atoms decreases. In contrast, the flux demand J required for oxidation increases exponentially. At least a thousand times p^* is required to run the oxidation kinetics accordingly to the models. This is the estimated value to satisfy the singular oxygen demand at the beginning of the oxidation process. If this is not fulfilled, the growth profile describing the oxidation process will be distorted.

In the case where not enough anions are available, the value of J_d could not increase many times of J. It can be assumed that non-stoichiometric oxide can grow in the anion-deficient section; Eq. (13) remains valid if $K < c_0$. We can also make a rough estimation that the value of K increases linearly over a period of δ/n ($n = 2, 3 \ldots$) growth until it reaches the value of c_0. Substituting in Eq. (3), we get a third degree expression at $x \approx 0$:

$$\frac{L}{x} - J = c_0 \frac{x}{\delta/n} \frac{dx}{dt}. \tag{25}$$

Integrating and returning to the normalized from of Eq. (18):

$$t_{(3)} = t_{(2)} - \frac{\alpha n}{\delta} x^2 + \frac{3}{2} \alpha n \delta, \quad 0 < x < \frac{\delta}{n}. \tag{26}$$

Approaching at $x \approx 0$:

$$t_{(3)} = \frac{n}{3} \frac{\alpha}{\delta^2} x^3. \tag{27}$$

This cubic dependence ($t_{(2)}$ and $t_{(3)}$ denote parabolic (Eq. (16)) and cubic dependences, respectively) appears in the initial stage of heat treatment at 700 K. When the growth reaches a stage such that $J < J_{ox}$, a stoichiometric layer grows according to Eq. (14). All this can be observed by the refractive index values (Figs. 5 and 6). It seems to be proven that if the heat treatment persists for the time predictable as $\alpha\delta$, in the second half of the annealing process the excess oxygen could be involved in the oxidation of the zirconium excess in the non-stoichiometric range. For the heat treatment at 700 K, Eq. (27) can be fitted by choosing $n \approx 500$. This means that the thickness of the transient layer is approximately 1 nm — thus, the change from Zr to
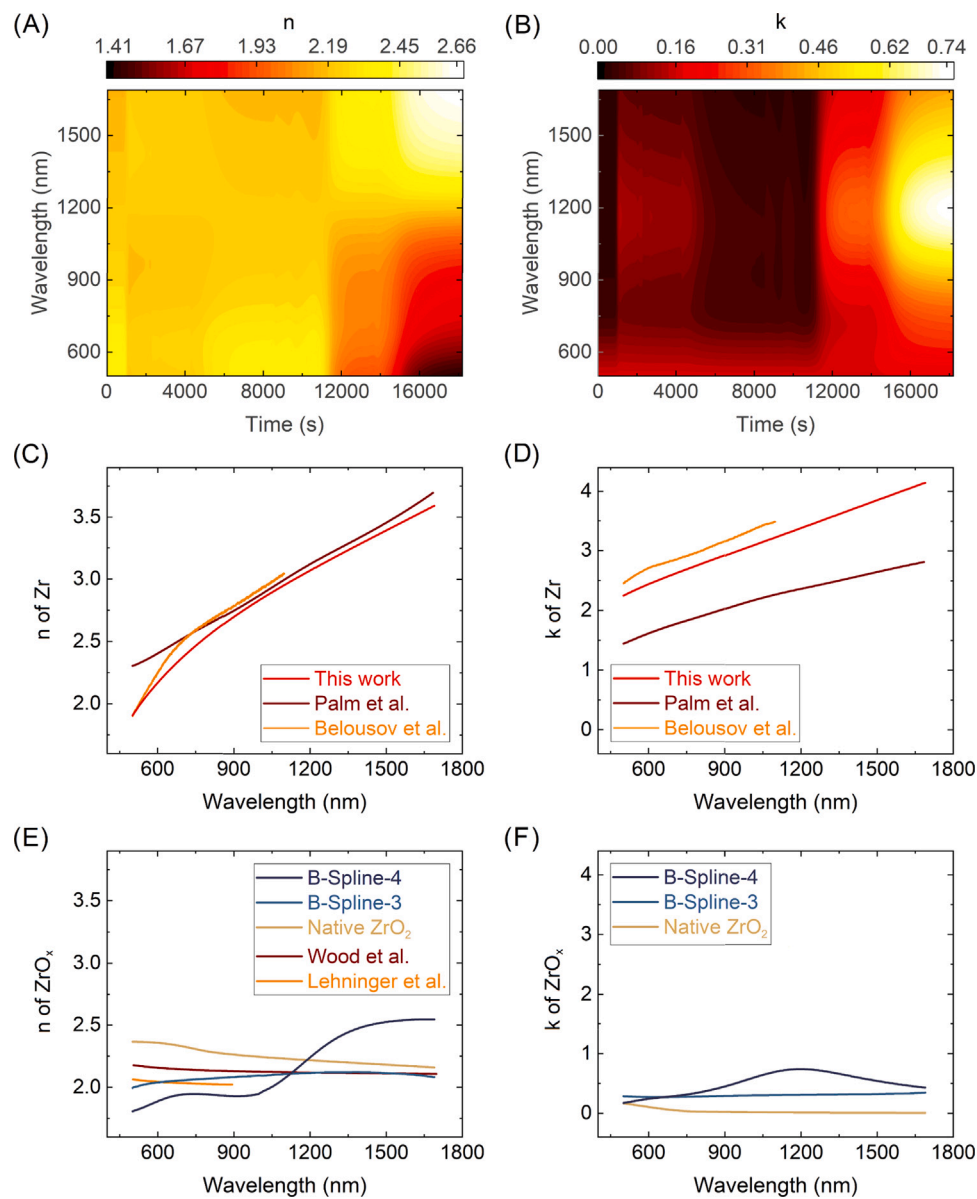
Fig. 3. Refractive index, *n*, (A) and extinction coefficient, *k*, (B) (spectra plotted along the vertical axes) as a function of time during the oxidation. *n* and *k* spectra of the substrate (Zr, (C) and (D)) and the layer (ZrO_2, (E) and (F)) measured in frame of this study, together with a few relevant references from the literature [32,38–40].
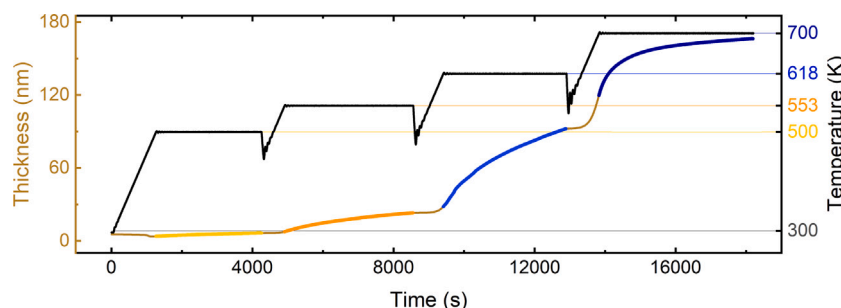

Fig. 4. Steps of thickness increase as a function of time under the influence of the increasing temperature values.

fully stoichiometric dioxide is rather abrupt. Our approximation seems to be absurd, but by treating the equations numerically we could get a more realistic value. On the other hand, Eq. (26) describing the final stage of the heat treatment process can be fitted with $n \approx 0.15$, which can be considered as $t_{(2)} = t_{(3)}$ identity — no transient layer is present.

This is not the only pressure-dependent effect that can affect the oxidation process. The pressure- and temperature-dependence can be analyzed by considering the standard free energy (ΔG) with a term corresponding to the so-called activity given in Ref. [43].
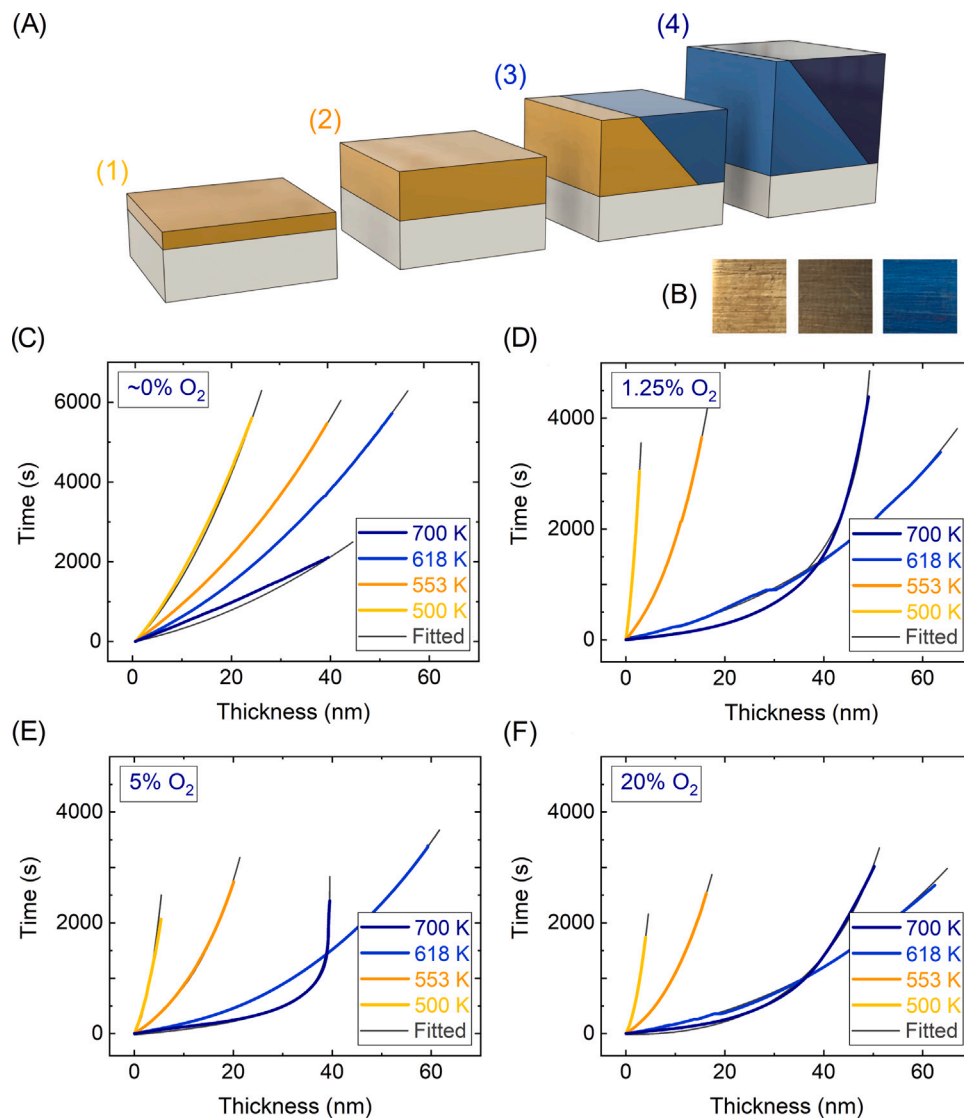
Fig. 5. (A) Optical models at different stages (1–4) of the oxidation process. (B) Photographs of ≈ 2 cm $\times$ 2 cm E125 alloy samples to demonstrate the change of color due to the different thicknesses of the oxides grown at various oxygen/argon ratios [23]. (C–F) Time versus thickness for different O_2 concentrations at different temperatures, determined from the optical model shown in (A). The solid dark-gray lines show the curves fitted using Eq. (14). In case of 700 K Eq. (26) was used instead.
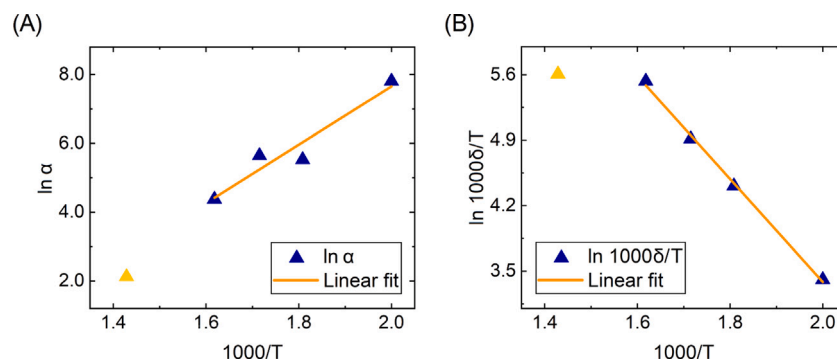

Fig. 6. Arrhenius plots of α (A) and δ/T (B). The yellow triangles belong to the temperature of 700 K, which is already outside of the defined 666 K upper limit defined, it can be seen that they do not fit well on the fitted lines.

The condition of chemical equilibrium is that the sum of the chemical potentials weighted by stoichiometric coefficients is zero. The oxygen pressure at which the oxidation starts can be calculated or used from the work of Ref. [44]. Based on the Ellingham diagram, about $p = 10^{-86}$ bar for p was estimated at $T = 600$ K.

The validity of the proposed model decreases with increasing thicknesses due to the vertical inhomogeneity of the oxide layer and the fluctuations in μ (the region of increasing deviation of the experimental and fitted curves in Fig. 5). Here, both the optical and the kinetic models have to be changed, possibly involving numerical methods. In

this region μ is not a single value anymore, but a spectrum and a function of the depth.

6. Conclusions

A simple phenomenological model was developed that attempts to relate the parameters of the transport properties of the atomic oxygen (anions) to the results of kinetics measured by ellipsometry in a thickness range (from a few nanometers to a few hundred nanometers) that has not yet been studied in detail. We have shown that the kinetic behavior can fenomenologically be described by the approach used for the analysis of p–n junctions in semiconductor physics. The equations postulate that the oxide thickness approaches a value determined by temperature. The resulting oxide is stoichiometric when the growth occurs in an oxygen-rich environment. Stoichiometry is temporarily impaired in an oxygen-deficient environment, but if the heat treatment time is long enough for $\alpha \cdot \delta$, it becomes complete by the excess oxygen present in the final stage of the process. The driving force introduced into our phenomenological model based on ellipsometric measurements determines the kinetics of growth in a consistent and concordant way.

CRediT authorship contribution statement

Alekszej Romanenko: Data curation, Formal analysis, Investigation, Visualization, Review editing. **Emil Agócs:** Data curation, Formal analysis, Investigation, Software. **Zoltán Hózer:** Conceptualization, Methodology, Review editing. **Peter Petrik:** Conceptualization, Data curation, Formal analysis, Funding acquisition, Investigation, Methodology, Writing of original draft, Review editing, Supervision. **Miklós Serényi:** Conceptualization, Formal analysis, Methodology, Writing of original draft, Review editing.

Declaration of competing interest

The authors declare that they have no known competing financial interests or personal relationships that could have appeared to influence the work reported in this paper.

Acknowledgments

Appendix A. Constants used in the calculations

- $k_B = 8.62 \cdot 10^{-5}$ eV/K, Boltzmann constant;
- $c_0 = 9.13 \cdot 10^{-19}$ mol/nm^3, O$^-$ concentration in ZrO$_2$;
- $K = c_0$ in units of mol/nm^3;
- $\theta = 666$ K.

Appendix B. Temperature dependence of parameters

See Table B.1.

- $\mu = 2.07 \cdot 10^3 \exp\left(\frac{-1.44}{k_B}\left[\frac{1}{T} - \frac{1}{\theta}\right]\right)$ m/(N· s), mobility;
- $D = \mu k_B T = 2.86 \ T \cdot 10^{-2} \exp\left(\frac{-1.44}{k_B}\left[\frac{1}{T} - \frac{1}{\theta}\right]\right)$ nm^2/s, diffusion coefficient;
- $J = 5.56 \cdot 10^{-20} \exp\left(\frac{-0.96}{k_B}\left[\frac{1}{T} - \frac{1}{\theta}\right]\right)$ mol/nm^2 s;
- $L = 2.61 \ T \cdot 10^{-20} \exp\left(\frac{-1.44}{k_B}\left[\frac{1}{T} - \frac{1}{\theta}\right]\right)$ mol/(nm s K);
- $\alpha = \frac{K}{J} = 16.4 \exp\left(\frac{0.96}{k_B}\left[\frac{1}{T} - \frac{1}{\theta}\right]\right)$ s/nm;
- $\delta = \frac{L}{J} = 0.47 \ T \exp\left(\frac{-0.48}{k_B}\left[\frac{1}{T} - \frac{1}{\theta}\right]\right)$ nm.

Table B.1
Calculated parameters of the kinetic curves at different temperatures. v_{drift} is provided for $x = \delta/2$.

T (K)	p^* (Pa)	δ (nm)	w (nm)	E (V/nm)	v_{drift} (nm/s)
666	2.580	313	11.0	$2.9 \cdot 10^{-3}$	$6.08 \cdot 10^{-2}$
618	0.680	156	9.5	$2.8 \cdot 10^{-3}$	$1.65 \cdot 10^{-2}$
553	0.076	27	6.2	$2.5 \cdot 10^{-3}$	$1.97 \cdot 10^{-3}$
500	0.008	15	5.0	$2.3 \cdot 10^{-3}$	$2.31 \cdot 10^{-4}$

References

[1] Y.L. Yao, Thermodynamics of parabolic time rate law of oxidation of metals, J. Chem. Phys. 43 (1965) 3050–3051.

[2] C. Wagner, Theoretical analysis of the diffusion processes determining the oxidation rate of alloys, J. Electrochem. Soc. (1952) 369–380.

[3] N. Cabrera, N.F. Mott, Theory of the oxidation of metals, Rep. Progr. Phys. 12 (1949) 163–184.

[4] Y. Unutulmazsoy, C. Cancellieri, M. Chiodi, S. Siol, L. Lin, L.P.H. Jeurgens, In situ oxidation studies of Cu thin films: Growth kinetics and oxide phase evolution, J. Appl. Phys. 127 (2020) 065101.

[5] A. Atkinson, Transport processes during the growth of oxide films at elevated temperature, Rev. Modern Phys. 57 (1985) 437–470.

[6] B. Cox, A Method for Calculating the Transient Oxidation of Zircaloys, Technical Report AECL–6784, Atomic Energy of Canada Ltd., 1980.

[7] E.A. García, Diffusion in a semi-infinite system with a moving interface at constant temperature for application to α-zirconium oxidation at high temperature, J. Nucl. Mater. 92 (1980) 249–256.

[8] V. Renčiuková, J. Macák, P. Sajdl, R. Novotný, A. Krausová, Corrosion of zirconium alloys demonstrated by using impedance spectroscopy, J. Nucl. Mater. 510 (2018) 312–321.

[9] A. Denis, E. Moyano, E.A. Garcia, Model to simulate high temperature oxidation kinetics of zircaloy-4: Parabolic and linear behaviour, J. Nucl. Mater. 110 (1982) 11–19.

[10] L. Zhang, L.-Y. Chen, C. Zhao, Y. Liu, L.-C. Zhang, Calculation of Oxygen diffusion coefficients in oxide films formed on low-temperature annealed Zr alloys and their related corrosion behavior, Metals (2019) 850.

[11] H.-I. Yoo, B.-J. Koo, J.-O. Hong, I.-S. Hwang, Y.-H. Jeong, A working hypothesis on oxidation kinetics of Zircaloy, J. Nucl. Mater. 299 (2001) 235–241.

[12] A. Lyapin, L.P.H. Jeurgens, P.C.J. Graat, E.J. Mittemeijer, Ellipsometric and XPS study of the initial oxidation of zirconium at room temperature, Surf. Inter. Anal. (2004) 989–992.

[13] A. Lyapin, L.P.H. Jeurgens, P.C.J. Graat, E.J. Mittemeijer, The initial, thermal oxidation of zirconium at room temperature, J. Appl. Phys. 96 (2004) 7126–7135.

[14] A. Lyapin, L.P.H. Jeurgens, E.J. Mittemeijer, Effect of temperature on the initial, thermal oxidation of zirconium, Acta Mater. (2005).

[15] D.L. Douglass, Carl Wagner, The oxidation of Oxygen-deficient Zirconia and its relationship to the oxidation of Zirconium, J. Electrochem. Soc. 113 (1966) 671.

[16] L.P.H. Jeurgens, A. Lyapin, E.J. Mittemeijer, The mechanism of low-temperature oxidation of zirconium, Acta Mater. (2005) 4871–4879.

[17] L.P.H. Jeurgens, A. Lyapin, E.J. Mittemeijer, The initial oxidation of zirconium—oxide-film microstructure and growth mechanism, Surf. Inter. Anal. 38 (2006) 727–730.

[18] G. Bakradze, L.P.H. Jeurgens, T. Acartürk, U. Starke, E.J. Mittemeijer, Atomic transport mechanisms in thin oxide films grown on zirconium by thermal oxidation, as-derived from 18o-tracer experiments, Acta Mater. 59 (2011) 7498–7507.

[19] E. Perez-Feró, T. Novotny, A. Pintér-Csordás, M. Kunstár, Z. Hózer, M. Horváth, L. Matus, Experimental results on the breakaway oxidation of the E110 cladding alloy under high-temperature isothermal conditions, Prog. Nucl. Energy 93 (2016) 89–95.

[20] T. Ahmed, L.H. Keys, The breakaway oxidation of zirconium and its alloys a review, J. Less Common Metals 39 (1975) 99–107.

[21] S. Leistikow, G. Schanz, Oxidation kinetics and related phenomena of zircaloy-4 fuel cladding exposed to high temperature steam and hydrogen-steam mixtures under PWR accident conditions, Nucl. Eng. Des. 103 (1987) 65–84.

[22] P. Petrik, A. Sulyok, T. Novotny, E. Perez-Feró, B. Kalas, E. Agocs, T. Lohner, D. Lehninger, L. Khomenkova, R. Nagy, J. Heitmann, M. Menyhard, Z. Hózer, Optical properties of Zr and ZrO2, Appl. Surf. Sci. 421 (2017) 744–747.

[23] P. Petrik, A. Romanenko, B. Kalas, L. Péter, T. Novotny, E. Perez-Feró, B. Fodor, E. Agocs, T. Lohner, S. Kurunczi, M. Stoica, M. Gartner, Z. Hózer, Optical properties of oxidized, hydrogenated, and native Zirconium surfaces for wavelengths from 0.3 to 25 μm - A study by ex situ and in situ spectroscopic ellipsometry, Phys. Status Solidi A (2019) 1800676.

[24] S. Zhao, F. Ma, K.W. Xu, H.F. Liang, Optical properties and structural characterization of bias sputtered ZrO2 films, J. Alloys Compd. 453 (2008) 453–457.

[25] M.A. Hopper, Anodic oxidation of Zirconium: Evidence of typical valve metal behavior, J. Electrochem. Soc. 124 (1977) 44.

[26] E.M. Patrito, Ellipsometric investigation of anodic Zirconium oxide films, J. Electrochem. Soc. 140 (1993) 1576.

[27] N.M. Bashara, Y.-K. Peng, Optical properties of Zircaloy and Zircaloy oxide by ellipsometry, Appl. Opt. 19 (1980) 3245.

[28] R.A. Synowicki, Thomas E. Tiwald, Optical properties of bulk c-ZrO2, c-MgO and a-As2S3 determined by variable angle spectroscopic ellipsometry, Thin Solid Films 455–456 (2004) 248–255.

[29] Martin Steinbrück, Nóra Vér, Mirco Groß e, Oxidation of advanced Zirconium cladding alloys in steam at temperatures in the range of 600–1200 °C, Oxid. Metals 76 (2011) 215–232.

[30] C. Proff, S. Abolhassani, C. Lemaignan, Oxidation behaviour of zirconium alloys and their precipitates – A mechanistic study, J. Nucl. Mater. 432 (2013) 222–238.

[31] H.H. Hsieh, W. Kai, R.T. Huang, M.X. Pan, T.G. Nieh, Effect of Zr-content on the oxidation and phase transformation of Zr-base amorphous alloys in air, Intermetallics 12 (2004) 1089–1096.

[32] D. Lehninger, L. Khomenkova, C. Roder, G. Gartner, B. Abendroth, J. Beyer, F. Schneider, D.C. Meyer, J. Heitmann, Ge nanostructures embedded in ZrO2 dielectric films for nonvolatile memory applications, ECS Trans. 66 (2015) 203–212.

[33] V.A. Markelov, V.V. Novikov, N.S. Saburov, A. Gusev, V.F. Kon'kov, M. Peregud, A.B. Dolgov, B.Yu. Volkov, V. Andersson, Irradiation test under advanced PWR conditions in the Halden reactor and post-irradiation examination of fuel rod claddings from different zirconium alloys, in: Presented on TopFuel 2018, 30 September – 4 October 2018, Prague, Czech Republic, 2018.

[34] K. Seeger, Semiconductor Physics, Springer-Verlag, 1973, p. 139.

[35] R. Kubo, The fluctuation-dissipation theorem, Reports on Progr. Phys 29 (1966) 255–284.

[36] Blaine Johs, Jeffrey S. Hale, Dielectric function representation by B-splines, Phys. Status Solidi A (2008) 715–719.

[37] D.V. Likhachev, On the optimization of knot allocation for B-spline parameterization of the dielectric function in spectroscopic ellipsometry data analysis, J. Appl. Phys. (2021).

[38] D.A. Belousov, V.P. Korolkov, V.N. Khomutov, R.V. Shimansky, R.I. Kuts, Determination of linewidth for metal/oxide gratings by measured diffraction efficiency in several orders, Proc. SPIE - Int. Soc. Opt. Eng. 11551 (2020).

[39] K.J. Palm, J.B. Murray, T.C. Narayan, J.N. Munday, Dynamic optical properties of metal hydrides, ACS Photon. 5 (11) (2018) 4677–4686, http://dx.doi.org/10.1021/acsphotonics.8b01243.

[40] D.L. Wood, K. Nassau, Refractive index of cubic zirconia stabilized with yttria, Appl. Opt. 21 (16) (1982) 2978–2981, http://dx.doi.org/10.1364/AO.21.002978.

[41] C. Krug, G. Lucovsky, Spectroscopic characterization of high *k* dielectrics: Applications to interface electronic structure and stability against chemical phase separation, J. Vacuum Sci. Technol. A 22 (2004) 1301–1308.

[42] S. Zhao, F. Ma, Z. Song, K. Xu, Thickness-dependent structural and optical properties of sputter deposited ZrO2 films, Opt. Mater. 30 (2008) 910–915.

[43] L.B. Pankratz, Thermodynamic Properties of Elements and Oxides, U.S.Department of the Interior, Bureau of Mines, 1982.

[44] H.J.T. Ellingham, Reducibility of oxides and sulphides in metallurgical processes, J. Soc. Chem. Indus. 63 (1944) 125–160.